PHOTONICS Research

THz-fiber waveguide composed of a biocompatible Vaseline core and Teflon holey cladding enabling a centimeter bending radius

Yong Soo Lee,[1,2,†] Inhee Maeng,[3,†] Mingyu Lee,[1,2] Seokjin Kim,[1,2] Chul Kang,[4] Daniele Tosi,[5] Soeun Kim,[4,7] Seung Jae Oh,[3,8] and Kyunghwan Oh[1,6,*]

[1]Department of Physics, Yonsei University, Seoul 03722, Republic of Korea
[2]Center for Quantum Technology, Korea Institute of Science and Technology, Seoul 02792, Republic of Korea
[3]YUHS-KRIBB Medical Convergence Research Institute, College of Medicine, Yonsei University, Seoul 03722, Republic of Korea
[4]Integrated Optics Laboratory, Advanced Photonics Research Institute, GIST, Gwangju 61005, Republic of Korea
[5]Department of Electrical and Electronical Engineering, Nazarbayev University, 010000 Astana, Kazakhstan
[6]Department of Physics, School of Sciences and Humanities, Nazarbayev University, 010000 Astana, Kazakhstan
[7]e-mail: sekim@gist.ac.kr
[8]e-mail: issac@yuhs.ac
[†]These authors contributed equally to this work.
*Corresponding author: koh@yonsei.ac.kr

Received 21 October 2024; revised 19 May 2025; accepted 21 May 2025; posted 27 May 2025 (Doc. ID 545598); published 1 August 2025

In this study, we introduce and experimentally validate, to our knowledge, a new type of terahertz (THz) fiber waveguide. The waveguide features a core made from petroleum jelly (commonly known as Vaseline) and a cladding made of holey polytetrafluoroethylene (PTFE), also known as Teflon. Since the core is biocompatible and the cladding is safe for human use, this design has promising applications for biocompatible probes in the THz range. We rigorously analyzed the transmission properties of the waveguide using the finite element method (FEM) and followed up with experimental validation using a THz time-domain spectroscopy (THz-TDS) system. The fiber supports single-mode operation for frequencies below 0.9 THz and demonstrates low-loss transmission of THz waves, even when tightly bent. For instance, with a bending radius as small as 1.61 cm, the fiber exhibited minimal losses of 0.23 dB/cm at 0.2 THz and 0.27 dB/cm at 0.5 THz, surpassing previous technical limitations. Another key advantage is the strong confinement of the THz waves within the petroleum jelly core, which helps maintain low dispersion and ensures stable pulse transmission, even under tight bends. The exceptional stability and flexibility of this biocompatible THz fiber make it highly suitable for sensing and imaging applications in confined, flexible environments, including potential uses within the human body.

https://doi.org/10.1364/PRJ.545598

1. INTRODUCTION

Recent advancements in terahertz (THz) technology have established its importance in nondestructive testing (NDT), especially in industries like semiconductors, plastics, and ceramics [1,2]. Its interaction with water molecules has also extended its use to biomedical sensing and imaging [3–5]. By detecting variations in water content, THz waves can accurately identify anomalies in biological tissues, such as tumors with high water concentrations, making it a valuable tool for tumor diagnostics [6–8]. THz technology's medical applications range from diagnosing skin cancers to detecting issues in deeper tissues, such as the mammary glands, oral cavities, and gastric lining [9–15]. Devices like handheld scanners and endoscopes have been developed to facilitate its clinical use in detecting internal malignancies [16].

There is a growing need for advanced THz probes that combine high-resolution imaging with flexibility for minimally invasive surgeries in tight spaces [15,17–21]. These constraints have increased demand for THz waveguides that maintain optimal transmission even with tight bends. THz technology is also expected to play a key role in non-invasive microsurgical procedures, such as intracranial endoscopies and robotic surgeries within confined spaces [20,21]. This underscores the need for waveguides that can sustain transmission with bending radii as small as 1 cm.

Several THz waveguide designs have been explored, including hollow metal waveguides [22–24], metal wires [25],

dielectric tubes [26,27], parallel metal plates [28,29], porous-core fibers [30–32], and photonic crystal fibers [33–35]. Each offers advantages and drawbacks. Metal waveguides, for instance, perform well but suffer losses under moderate bending, while hollow waveguides have lower transmission loss due to reduced material absorption but face challenges with wave confinement. Solid-core fibers provide better wave confinement but struggle with material absorption [36].

In this study, we designed and validated a composite THz fiber optimized for transmission with significantly reduced bending loss, achieving a bending radius of ~10 mm. The fiber consists of polytetrafluoroethylene (PTFE) cladding with 19 hexagonally arranged air holes, and a petroleum jelly (Vaseline) core. Both the holey PTFE cladding and Vaseline core are biocompatible [37] and exhibit low THz absorption. This unique combination resulted in a novel waveguide with strong bending resilience, minimizing attenuation across the 0.2–0.9 THz frequency range. To our knowledge, this is the first THz waveguide to maintain high transmission at a tight bending radius of 16.1 mm. We performed finite element method (FEM) simulations to optimize the waveguide's properties and confirmed its low bending loss through experimental testing using THz time-domain spectroscopy (THz-TDS).

2. PROPOSED WAVEGUIDE STRUCTURE AND NUMERICAL ANALYSES

Figure 1 illustrates schematic concepts of the proposed THz fiber. On the left of the figure, the cross-sectional design of the THz fiber is shown, highlighting its structural parameters. The core, cladding region, and air holes are denoted by yellow, blue, and white colors, respectively.

The proposed waveguide consists of a hexagonally arranged PTFE (polytetrafluoroethylene) holey cladding with a Vaseline-filled core. At THz frequencies, Vaseline and PTFE have refractive indices of 1.5 and 1.447, respectively, as reported in Refs. [31,38]. The waveguide functions similarly to traditional step-index glass fibers, relying on total internal reflection between the Vaseline core and the PTFE cladding. The effective refractive index of the cladding can be fine-tuned by adjusting the configuration of the air holes [39].

The PTFE cladding was fabricated using established methods [39], and the key structural parameters are as follows: the air hole diameter (D) is 430 μm, the spacing between holes (Λ) is 560 μm, and the overall external diameter (O.D.) is 3 mm. The Vaseline core has the same diameter as the air holes ($D = 430$ μm). This composite structure is designed to enhance mode confinement, leading to more stable THz transmission even during tight fiber bending. Figure 1 illustrates the azimuth angle (φ), which references the plane of bending, along with a schematic representation of the fiber's bending performance. For a tight bending radius of ~10 mm, the fiber maintained nearly the same intensity profile, and the output in both temporal and spectral domains remained consistent with the initial distributions, as schematically shown in Fig. 1.

To systematically assess the fiber's performance under bending and its ability to guide THz waves, finite element method (FEM) simulations were performed using COMSOL Multiphysics software. Figure 2 presents the electric field magnitude distribution of the fundamental mode across the fiber's cross-section. In Fig. 2(a), the bending performance of the proposed fiber is compared to that of a conventional step-index solid cladding fiber (SI-SCF), both using a Vaseline core with a diameter of 430 μm and PTFE cladding. Tests were conducted at a frequency of 0.5 THz, with the bending radius (R) varied between 20 and 200 mm, corresponding to curvatures (C) ranging from 5 to 50 m^{-1}. The bending direction was set to $\varphi = 0°$, and the results showed distinct differences in THz wave confinement between the two fiber designs. In conventional single-mode SI-SCFs used for telecommunications, the core diameter-to-wavelength ratio is typically maintained between 4:1 and 7:1 [39] to ensure sufficient modal confinement. For the terahertz (THz) spectral region, the wavelength corresponding to 1.0 THz is approximately 300 μm. This implies that a conventional SI-SCF designed for single-mode operation would require a core diameter of over 1 mm. Consequently, the total fiber outer diameter would reach over 1 cm, making it difficult for the fiber to bend. In this study, we

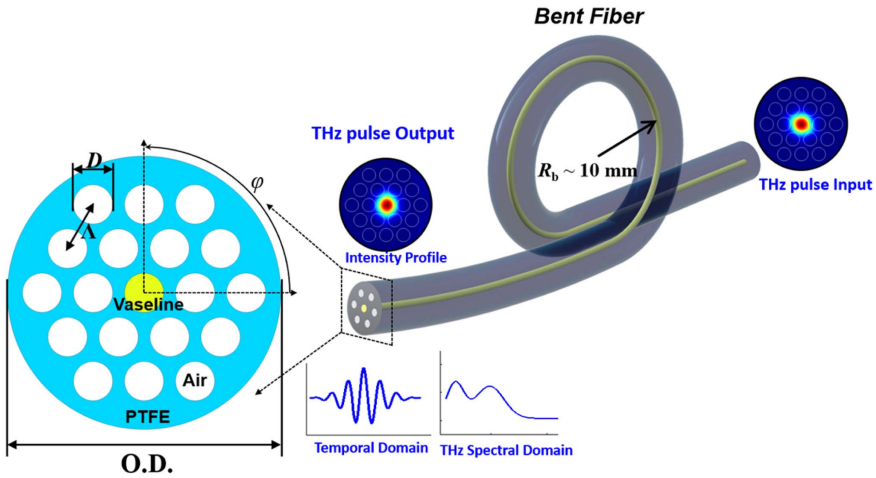

Fig. 1. Transverse cross-section of the proposed THz fiber composed of Vaseline core and PTFE holey cladding (O.D.: outer diameter, D: air hole diameter, Λ: air hole pitch, φ: azimuth angle referenced to the bending orientation).

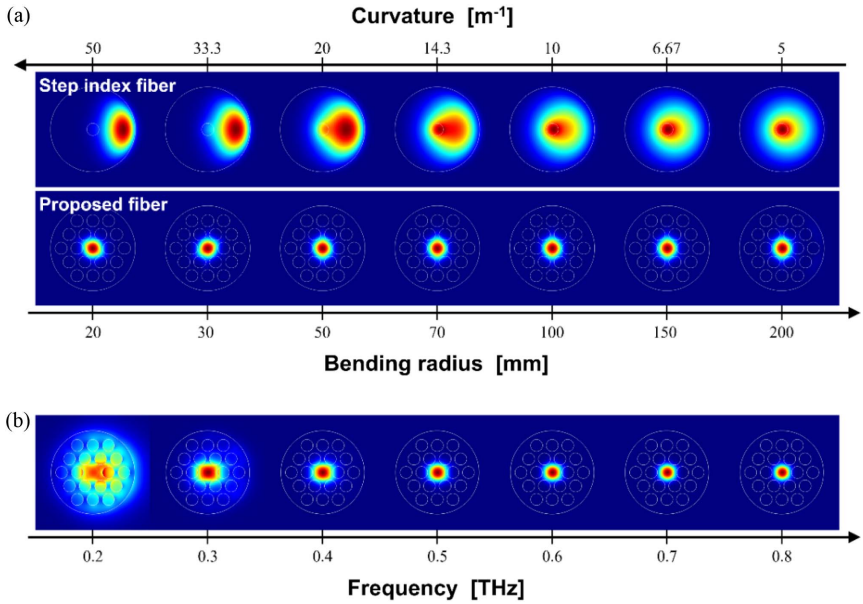

Fig. 2. Spatial distributions of the electric field magnitude of the fundamental mode. (a) Comparison of the proposed fiber with step index solid cladding fiber (SI-SCF) for various bending radii $R = 20$ to 200 mm at the frequency of 0.5 THz. Here, the bending angle $\varphi = 0°$. (b) Change of the fundamental mode's spatial intensity distribution with the frequency when the bending radius $R = 30$ mm.

set the core and cladding diameters of both the SI-SCF and the proposed fiber to be identical, for clear comparison. The core diameter was 430 μm, and the outer diameter was 3 mm. The SI-SCF employed a solid PTFE cladding, whereas the proposed fiber featured a holey PTFE cladding consisting of 19 air holes (each 430 μm in diameter) arranged in a hexagonal lattice. This holey cladding allowed a smaller core diameter-to-wavelength ratio of ∼1:1, which was impossible in conventional SI-SCF.

In the SI-SCF, the THz wave shifts away from the core when the bending radius falls below 50 mm, resulting in significant bending losses. In contrast, the proposed fiber, with air holes embedded in its cladding, retains core guidance even at smaller bending radii. This suggests that the proposed fiber offers superior bending resilience compared to the SI-SCF, thanks to enhanced modal confinement. The strong refractive index contrast between the Vaseline core and the air-hole cladding contributes to this improved performance, as discussed in Ref. [38].

Figure 2(b) examines the response of the fundamental mode to frequency variations from 0.2 to 0.8 THz, keeping a constant bending radius of $R = 30$ mm at $\varphi = 0°$. This frequency range is particularly relevant for emerging biomedical applications, as noted in Refs. [2,6]. At the lower frequency of 0.2 THz, the mode spreads into the holey cladding, indicating a potential increase in bending losses as more of the THz wave leaks from the core. However, at frequencies above 0.4 THz, the proposed fiber effectively confines the THz wave within the core, demonstrating its potential to reduce bending losses. Figure 2 highlights the fiber's superior THz guidance and improved resilience to bending. It is worth noting that bending at $\varphi = 30°$ and 90° produces identical results, as does bending at $\varphi = 0°$ and 60°, due to the symmetric hexagonal arrangement of the air holes.

The propagation characteristics of THz electromagnetic waves in the proposed fiber were thoroughly analyzed, focusing on the effective index, dispersion, material loss, and confinement loss of the guided modes. Figure 3 presents the results, comparing a straight fiber to a bent fiber with a 30 mm radius at $\varphi = 0°$. To simulate the effects of bending, we used geometrically exact beam theory (GEBT), which produced an equivalent step-index profile, offering a theoretical framework for understanding how bending alters the fiber's optical properties [40,41].

To assess the effective index of the fiber's cladding modes, a space-filling method was applied across the THz frequency range of 0.2 to 1.2 THz. The cut-off frequency for the first higher-order mode was estimated by identifying where the effective indices of the guided modes intersect with that of the cladding mode [39]. Figure 3(a) shows the effective indices for the first few guided modes: the cladding mode (gray line), the fundamental mode in a straight fiber (black line), the fundamental mode in a bent fiber with a 30 mm radius (red line), and the first excited mode (blue line). The intersection of the gray and blue lines marks the cut-off frequency for the first excited mode, which occurs at approximately 0.9 THz. This indicates that the fiber can operate in single mode for frequencies below 0.9 THz, including the critical THz band around 0.45 to 0.5 THz, which is particularly useful for biomedical applications where water's high absorption and reflection properties are beneficial [42,44].

Moreover, the stability of the effective index for the fundamental mode in the bent fiber across the 0.4 to 0.9 THz range, despite the 30 mm bending radius, suggests that the core functionality remains intact even under significant bending. This is a key advantage for practical applications, especially in the biomedical field, where both flexibility and reliable performance are essential.

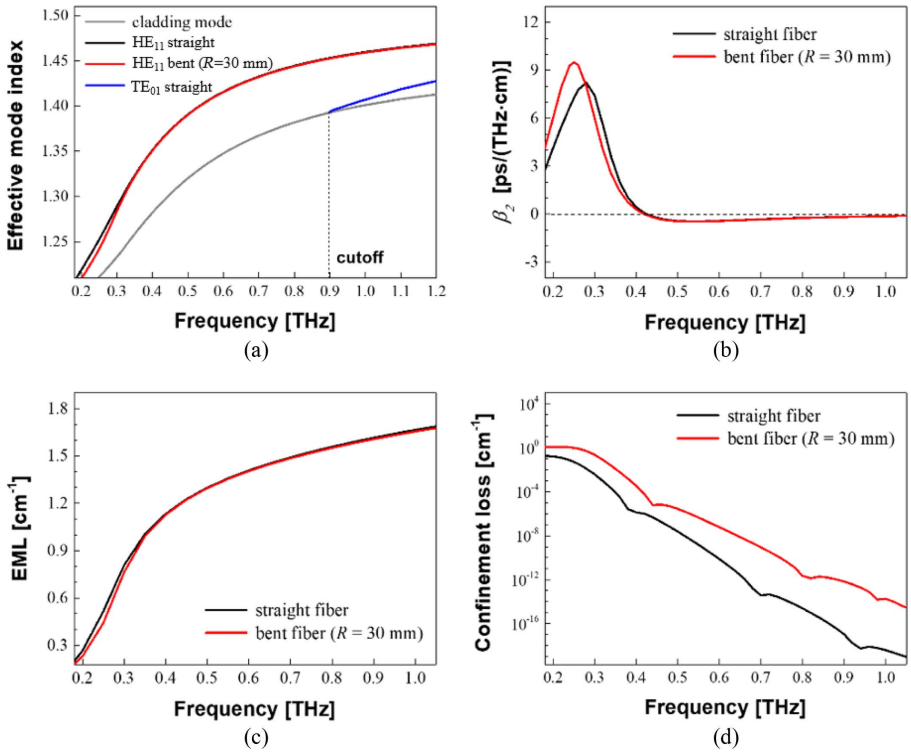

Fig. 3. Optical properties of the proposed THz fiber: (a) effective mode index and single-mode condition, (b) dispersion, (c) effective material loss, and (d) confinement loss.

Figure 3(b) shows the dispersion characteristics of the fundamental mode of the fiber. Dispersion is expressed by the following equation, which utilizes the effective index of the mode, $n_{\text{eff}}(\omega)$ [39]:

$$\beta_2 = \frac{2}{c}\frac{\mathrm{d}n_{\text{eff}}}{\mathrm{d}\omega} + \frac{\omega}{c}\frac{\mathrm{d}^2 n_{\text{eff}}}{\mathrm{d}\omega^2}\,[\text{ps}/(\text{THz}\cdot\text{cm})]. \tag{1}$$

Here $\omega = 2\pi f$. For $f > 0.4$ THz, the dispersion shows negligible change against bending. In the frequency range, the average dispersion of the proposed fiber was estimated to be $\beta_{2\text{avg}} = -0.23 \pm 0.22$ ps/(THz · cm), which was close to zero with a small fluctuation. We noted that β_2 at $f = 0.5$ THz was −0.48 ps/(THz · cm). Vaseline and PTFE show little change in the refractive index, in the frequency range of 0.2 to 1.1 THz [31,38]. Hence, the material dispersion is negligible, and the waveguide dispersion becomes a dominant contribution to β_2 [31]. In contrast, for $f < 0.4$ THz, β_2 of the bent fiber showed conspicuous differences. This is consistent with Fig. 2(b), where the mode distribution significantly extends to the cladding at the low-frequency region. This modal guidance altered the effective index of the mode when the fiber was bent to result in notable changes in the dispersion for $f < 0.4$ THz in Fig. 3(b).

Next, we examined two key optical loss mechanisms in the proposed fiber. The first is effective material loss (EML), which arises from the absorption properties of the materials used in the fiber. We specifically considered the THz absorption data for Vaseline and PTFE [45,46]. The second mechanism is confinement loss (L_c), which occurs when the mode leaks from the core into the cladding [39].

To evaluate EML, we analyzed the overlap between the guided mode and the materials in both the core and cladding, as outlined in Eq. (2) [31,47]. This approach allowed us to quantify how much of the THz wave interacts with the absorbing materials, giving insight into the fiber's performance under practical conditions:

$$\text{EML} = \frac{(\varepsilon_0/\mu_0)^{1/2}}{2\int_{\text{All}} S_z \mathrm{d}A}\left(\int_{A_{\text{core}}} n_{\text{core}}\alpha_{\text{core}}|E|^2 \mathrm{d}A_{\text{core}} + \int_{A_{\text{cladding}}} n_{\text{cladding}}\alpha_{\text{cladding}}|E|^2 \mathrm{d}A_{\text{cladding}}\right)[\text{cm}^{-1}], \tag{2}$$

where ε_0 and μ_0 are the vacuum permittivity and the permeability. n_{core} and n_{cladding} are the refractive indices of Vaseline and PTFE, respectively; α_{core} and α_{cladding} are the material absorption [31,37]. S_z is the axial component of the Poynting vector calculated for the fundamental mode; $|E|$ is the magnitude of the electric field of the mode. In Fig. 3(c) EML showed a negligible difference when the fiber was bent for $f > 0.4$ THz, and EML was estimated to be 1.30 cm^{-1} at $f = 0.5$ THz. For $f < 0.4$ THz, the bent fiber's EML decreased slightly, which is attributed to the mode extension into PTFE holey cladding, where the air material absorption is lower.

The confinement loss of the proposed fiber is shown in Fig. 3(d). The confinement loss, L_c, was calculated using the equation [38]

$$L_c = \left(\frac{4\pi f}{c}\right) \mathrm{Im}(n_{\mathrm{eff}})\,[\mathrm{cm}^{-1}], \tag{3}$$

where $\mathrm{Im}(n_{\mathrm{eff}})$ is the imaginary part of the complex effective index of the fundamental mode, and c is the speed of light. When the fiber is bent, the confinement loss increases by a few orders of magnitude in the entire THz frequency range, as shown in Fig. 3(d). However, the magnitude of L_c was insignificant compared to EML, and therefore, the transmission loss of the proposed fiber was mainly attributed to EML obtained in Fig. 3(c). The findings in Fig. 3 suggest that a Vaseline core coupled with a holey PTFE cladding is optimal for THz biomedical applications due to its support for single-mode guidance, low absorption, flexibility, and biocompatibility.

3. FABRICATION OF VASELINE CORE PTFE HOLEY CLADDING THz FIBERS

The custom-ordered polytetrafluoroethylene (PTFE) holey fiber, detailed in Fig. 1 with an outer diameter (O.D.) of 3 mm, pitch (Λ) of 560 μm, and hole diameter (D) of 430 μm, was acquired as per specifications [48]. The variation of these parameters along ∼100 mm fiber was negligible, less than 1%. As illustrated in Fig. 4, a unique fabrication process was employed in which only the central hole of the fiber was filled with Vaseline. This was achieved by sealing the peripheral holes with UV-curable polymers [49], thereby directing the Vaseline exclusively into the central hole. The filling process involved submerging the fiber in a container of Vaseline heated to 140°C to reduce its viscosity, facilitating its uptake into the fiber's central hole via syringe-induced negative pressure. This process was meticulously controlled, maintaining a filling rate of approximately 1 cm length of fiber for 10 min to prevent the formation of air bubbles within the core. Following the Vaseline's jellification at room temperature, we produced fibers of approximately 90 mm in length. The fiber ends were then cleaved with a razor in preparation for experimental use.

The cross-sectional microscope image of the finished fiber, shown in the right inset of Fig. 4, confirms the successful core filling. At room temperature, the Vaseline core's refractive index is approximately $n_{\mathrm{core}} \sim 1.5$, with a material absorption coefficient of ∼2 cm^{-1} [38], while PTFE exhibits a refractive index of ∼1.447 [31]. This combination of materials and the precise fabrication technique resulted in a fiber structure optimized for THz wave guidance, as required for the intended experimental investigations.

4. THz TRANSMISSION MEASUREMENTS

We used a fiber-coupled THz time-domain spectroscopy (TDS) system to characterize the transmission characteristics of the proposed fiber [31]. THz pulses were generated using a femtosecond laser with a center wavelength of 1560 nm and pulse width of 80 fs (Menlosystems ELMA). The femtosecond laser was guided to the transmitter (Tx) and receiver (Rx) antenna (Menlosystems TERA 15-TX-FC and TERA 15-RX-FC) by silica optical fiber patch cords. The generated THz pulses were sent to two TPX lenses with a focal length of 5 cm and coupled to our THz fiber. THz pulses passing through our fiber were collected to the receiver antenna by using two TPX lenses with a focal length of 5 cm. The experimental setup for bending characteristics is shown in Fig. 5. The fiber used in the experiment was ∼86 mm long, and both ends were fixed by mechanical mounts.

The fiber was mounted between two fixtures, "Holder 1" and "Holder 2." The distance between the mounts was $L_s \sim 46$ mm when the fiber was straight. The transmitter (Tx) and receiver (Rx) were connected at each fiber end using TPX lens pairs. The entire setup was placed on a goniometer, which allowed rotation around a central point "O." To ensure repeatability in the bending experiments, "Holder 2" was specially designed to enable the test on fiber to move back and forth along its axis through a hole in the holder. In contrast, "Holder 1" remained fixed throughout the experiments. As the bending angle θ increased, the distance between "Holder 2" and the receiver-side end of the fiber changed—from an

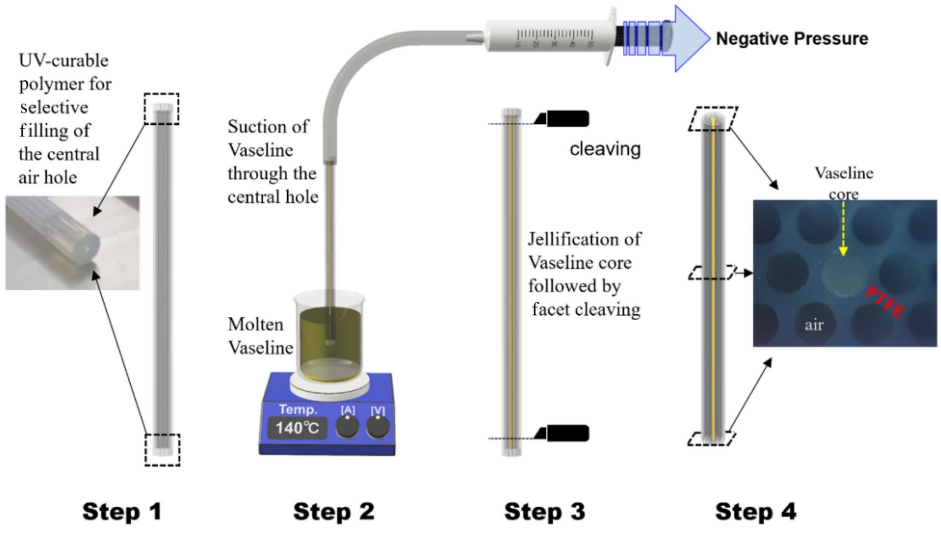

Fig. 4. Fabrication processes of the proposed composite THz fiber.

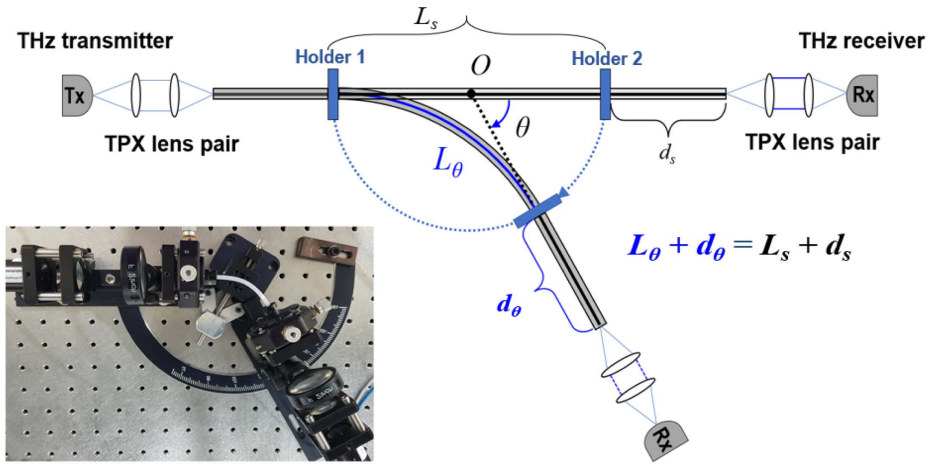

Fig. 5. Experimental setup to measure the bending characteristics of the proposed THz fiber. The fiber was mounted on a goniometer, and bending parameters are the radius of curvature C, goniometer angle θ, and bent fiber length L_θ. THz pulses passed through the proposed fiber and were detected in the time domain. As the fiber bends, the fiber passes through Holder 2, to make d_θ longer than d_s. Therefore, L_θ decreases with increasing θ. Note that the straight fiber has L_s and d_s for $\theta = 0°$.

initial distance d_s (for the straight fiber) to d_θ (for the bent fiber), with $d_\theta > d_s$. To maintain a constant total fiber length, the fiber segment length L_θ between the holders had to decrease accordingly, satisfying the condition $L_\theta + d_\theta = L_s + d_s$, where L_s is the straight fiber length between the holders. Holder 2 was rotated on a goniometer at an angle $0° \le \theta \le 110°$, which resulted in variable fiber path length L_θ, bending radius R, and the corresponding curvature C. To ensure reliable THz signal collection under fiber bending, the optical alignment at the receiver side was carefully adjusted for each bending condition. Table 1 summarizes those parameters used in experiments. L_θ decreased from 46 mm (straight fiber $\theta = 0°$) to 30.9 mm (bent fiber $\theta = 110°$).

Traces of the THz pulses that arrived at the receiver are shown in Fig. 6 in the time domain for various bending parameters. Here, we bent the fiber on two planes in the horizontal direction $\varphi = 0°$ and the vertical direction $\varphi = 90°$. See Fig. 1. As the bending radius R decreased, the fiber path length L_θ decreased to make the THz pulse arrive earlier, consistent with prior reports.

The proposed fiber showed very stable THz transmission characteristics even under tight bending conditions of $R \sim 1$ cm but showed distinctive responses to the direction of bending. In the case of horizontal bending, as shown in Fig. 6(a), the proposed fiber did not show noticeable degradation in the signal strength or the pulse duration. The peak-to-peak value of the THz pulses remained nearly the same as the straight case, even at $R = 16.1$ mm or $C = 62.1$ m^{-1}. Fiber bending in the vertical direction, in contrast, reduced the signal strength, as shown in Fig. 6(b). Especially, the front part of the THz pulse decreased noticeably for a tighter bending radius. The vertical bending introduces the field leakage more toward PTFE, as shown in Fig. 1, which might be under the influence of structural changes induced by the bending. This asymmetric leakage of the guided mode into the holey cladding in bent holey fibers has been observed in other spectral ranges [50], which can be further suppressed by an optimal arrangement of air holes [51]. Nevertheless, we confirmed that the low loss and low dispersion of the proposed fiber are mainly attributed to the excellent bending performances of the proposed THz fiber in Fig. 6(a).

Table 1. Bending Parameters for the THz Fiber

Angle, θ	R [mm]	C [m^{-1}]	L_θ [mm]
0°	–	–	46.0
30°	85.8	11.7	44.9
60°	39.8	25.1	41.7
90°	23.0	43.5	36.1
110°	16.1	62.1	30.9

Table 2 compares the dispersion characteristics of the proposed Vaseline core PTFE holey cladding fiber with those reported in prior studies, based on fiber type and core material. The dispersion characteristics were calculated based on the relationship between $\Delta\tau$, Δf, and L, using data presented in each study. Here, $\Delta\tau$ represents the temporal spread of the pulse (ps), Δf denotes the width of the frequency spectrum within the pulse (THz), and L is the length of the optical fiber (cm). Generally, dispersion tends to be lower when the core is composed of air or exhibits a porous structure with a high air content. Despite possessing a solid-state core, the proposed optical fiber demonstrates dispersion levels that are similar to or lower than those of a porous core. This suggests that the Vaseline core may offer advantageous dispersion properties compared to other materials.

We further investigated the transmission characteristics of the proposed THz fiber in the frequency domain to locate the low-loss window. The transmittance of the straight fiber is shown in Fig. 7(a). Here, the transmittance was obtained as P_{out}/P_{in}, where P_{in} and P_{out} are the power before being incident on the optical fiber and the power after passing through the optical fiber, respectively. We also quantified the transmission loss (TL) in the conventional unit of dB/cm:

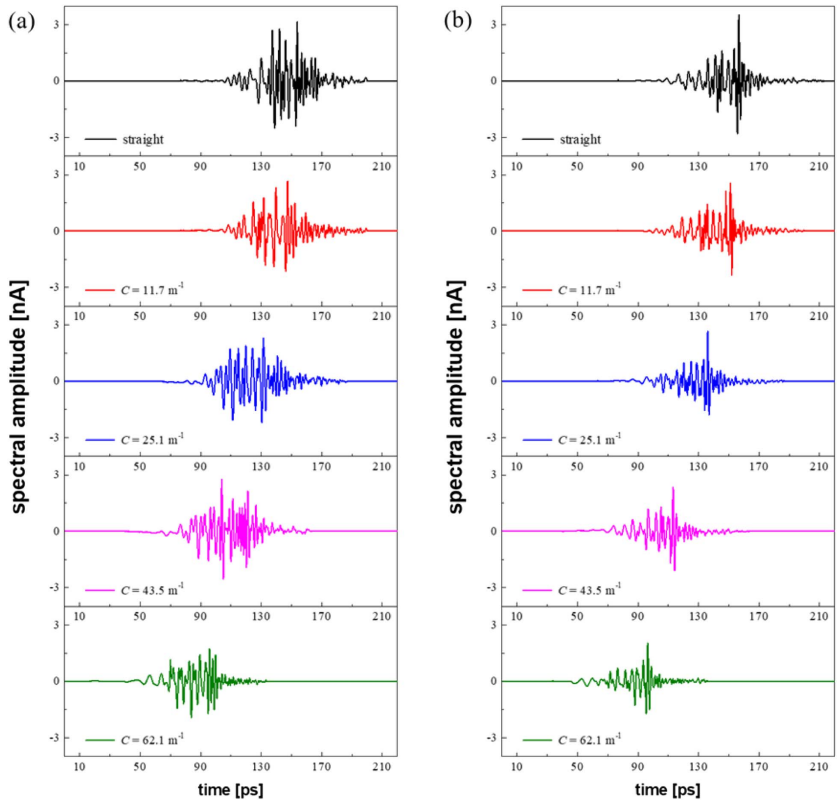

Fig. 6. Measurement of THz pulses through the proposed fiber in the time domain: (a) when the fiber was bent horizontally, $\varphi = 0°$ and (b) vertically, $\varphi = 90°$.

Table 2. Comparison of the Proposed THz Fiber with Prior Reports[a]

Reference	Fiber Type	Material		Length [cm]	Dispersion [ps/(THz·cm)]
		Core	Cladding		
[25]	Two-wire waveguide	Air	Air	9.5	4.0[b]
[29]	Parallel plate waveguide	Air	Air	1.6	1.5[b]
[31]	Porous-core fiber	PTFE	Air	20	1.9[b]
[32]	Porous-core fiber	PE + PMMA	Air	33.5	13.9[b]
[33]	Porous-core PCF	COC	Holey COC	5	10.5[b]
[35]	Photonic crystal fiber	HDPE	Holey HDPE	2	9.0[b]
Proposed	Holey cladding fiber	Vaseline	Holey PTFE	9	6.0[b]
					6.5[c]

[a]The dispersion ($= \Delta\tau/\Delta f L$) was estimated from the data presented in each study.
[b]Straight condition.
[c]Bent condition.

$$\mathrm{TL} = \frac{10}{L}\log\left(\frac{P_{\mathrm{in}}}{P_{\mathrm{out}}}\right)[\mathrm{dB/cm}], \tag{4}$$

where L is the length of the proposed fiber, and we estimated TL using a cut-back method [38]. The proposed fiber reached high transmittance peaks of more than 60% near $f = 0.2$ and 0.5 THz, as indicated by arrows in Fig. 7(a). The corresponding TL was ~0.18 dB/cm at $f = 0.2$ THz and ~0.26 dB/cm at $f = 0.5$ THz, which could serve as a dual-band window. The latter low-loss window holds practical importance since it is the water interaction band $f = 0.45$–0.5 THz, where water's high absorption and reflection can be advantageous [42,44] for biomedical applications. In the frequency range $f > 0.5$ THz, the transmittance decreased rapidly, which is attributed to the material absorption of PTFE [31]. In the frequency range 0.2 THz $< f <$ 0.9 THz, where the proposed fiber operates in the single mode, as shown in Fig. 3(a), the highest TL was estimated to be ~0.99 dB/cm.

We also confirmed the bend resilience of the proposed THz fiber in the frequency domain in Fig. 7(b), where the transmittance ratio of the bent fiber to the straight fiber is plotted for various curvatures. In a wide frequency band of 0.2 THz $< f <$ 0.9 THz where the single-mode guidance is satisfied as in Fig. 3(a), the proposed fiber maintained a very

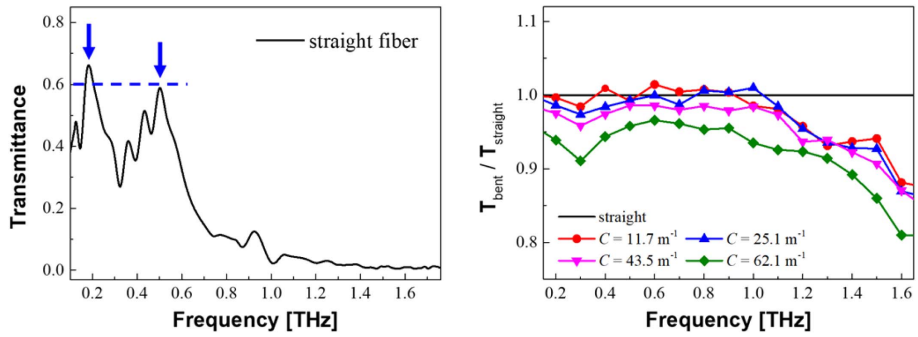

Fig. 7. Transmittance of the proposed fiber in the THz frequency domain: (a) transmittance of a straight fiber; (b) transmission ratio of the bent fiber to the straight fiber for various curvatures.

Table 3. Comparison of the Proposed THz Fiber with Prior Reports

Reference	Fiber Type	Material		Bending Radius [mm]	Operating Frequency [THz]	Loss [dB/cm]
		Core	Cladding			
[23]	Metal hollow fiber (tube)	Air	Silver (coated)	150	1.2–1.58	<0.08
[24]	Hollow fiber (tube)	Air	Silver/polypropylene	150	0.3	<0.013
[26]	Hollow fiber (tube)	Air	PMMA	100	0.3–1.0	<0.5 cm^{-1}
[27]	Circular tube lattice fiber	Air	PMMA	100	0.25–1	<2
[31]	Porous-core fiber	PTFE	Air	210	0.2–0.33	<0.78
Proposed	Holey cladding fiber	Vaseline	Holey PTFE	16.1	0.2–0.9	0.18 @0.2 THz 0.22 @0.5 THz

high ratio over 0.9 even for tight bending at $C = 62.1$ m^{-1} or $R = 16.1$ mm, which also confirmed the excellent bending performance of the proposed fiber.

Table 3 compares key features of the proposed "Vaseline core PTFE holey cladding" fiber with the prior reports.

The proposed fiber sustained a high level of transmittance of ~60% at the tightest bending radius of 16.1 mm, as confirmed by Fig. 7. Notably, this bending radius represents nearly an order of magnitude improvement compared to previous works and is unachievable with conventional air-core fibers. The proposed fiber showed a higher transmission loss of TL < 0.99 dB/cm in the single-mode operation band of 0.2 THz < f < 0.9 THz. However, it showed two low-loss bands near $f = 0.2$ THz (TL ~ 0.18 dB/cm in straight fiber, ~0.23 dB/cm in bent fiber of $R = 16.1$ mm) and $f = 0.5$ THz (TL ~ 0.22 dB/cm in straight fiber, ~0.27 dB/cm in bent fiber of $R = 16.1$ mm). Note that the transmission loss of 0.23–0.27 dB/cm at a very tight bending radius of $R = 16.1$ mm has never been achieved, to the best knowledge of the authors. In a separate study, the authors have investigated a PTFE porous-core fiber without Vaseline filling [31]. In the study, PTFE with the hexagonal air hole array was assumed, similar to this work but it did not have the Vaseline-filled center hole. In Ref. [31] the entire holey PTFE was used as the porous core and surrounding air served as the cladding. This structure provided the single-mode guidance at a slightly lower frequency range, 0.2–0.33 THz, with a transmission loss of <0.78 dB/cm at a much larger bending radius of 210 mm. As shown in Fig. 8, the porous-core/air-clad fiber shows a noticeable transmission loss as the bending radius decreases from 32.3 cm to 20.8 cm, while the Vaseline core fiber maintains a high transmittance even at a much smaller bending radius of 1.61 cm. A combination of jelly-type Vaseline core and holey PTFE cladding was proven to be an effective solution for THz transmission under extreme bending conditions, enabling *in vivo* medical diagnosis and imaging systems.

5. CONCLUSION

Numerical simulations and experimental studies were conducted on a new type of THz optical fiber consisting of a Vaseline core and PTFE holey cladding to investigate their optical behaviors under extreme bending. The jelly nature of the Vaseline core was strategically utilized to enhance core confinement, enabling the fiber to guide THz waves effectively even when subjected to substantial bending. The fiber design was optimized to operate in a single-mode regime for a wide frequency band of 0.2 THz < f < 0.9 THz, and it demonstrated a noteworthy transmission capability, particularly at a bending radius as tight as $R = 16.1$ mm. Transmission losses for the fiber were quantified, and both in straight alignment and bent configuration, the fiber exhibited a notably low loss at two spectral positions, $f = 0.2$ THz and 0.5 THz. The lowest loss was achieved near $f = 0.2$ THz, ~0.18 dB/cm in straight fiber and ~0.23 dB/cm in bent fiber with $R = 16.1$ mm. Near the $f = 0.5$ THz mark, relevant for H_2O-absorption-based biomedical applications, the fiber showed a loss of ~0.22 dB/cm straight fiber, ~0.27 dB/cm bent fiber, with $R = 16.1$ mm. The deformation of the THz pulse in the time domain due to the bending in the horizontal direction was

minimal, underscoring the fiber's potential for applications requiring high transmission fidelity in strictly constrained environments. These transmission qualities make the fiber an excellent candidate for THz applications requiring reliable performance under strict bending constraints, such as *in vivo* biomedical procedures or integration into compact THz devices and systems.

Funding. Institute of Information Communications Technology Planning Evaluation (2022-0-01029, RS-2022-II221044); National Research Foundation (2023R1A2C1007165).

Acknowledgment. This work was supported by the BK-21 FOUR program through National Research Foundation of Korea (NRF) under Ministry of Education.

Disclosures. The authors declare no conflicts of interest.

Data Availability. Data underlying the results presented in this paper are not publicly available at this time but may be obtained from the authors upon reasonable request.

REFERENCES

1. I. Amenabar, F. Lopez, and A. Mendikute, "In introductory review to THz non-destructive testing of composite mater," J. Infrared Millim. Terahertz Waves **34**, 152–169 (2013).
2. S. Zhong, "Progress in terahertz nondestructive testing: a review," Front. Mech. Eng. **14**, 273–281 (2019).
3. I. Maeng, S. Lee, E. Q. Han, *et al.*, "Unusual terahertz-wave absorptions in δ/α-mixed-phase $FAPbI_3$ single crystals: interfacial phonon vibration modes," NPG Asia Mater. **13**, 75 (2021).
4. H. S. Bark, I. Maeng, J. U. Kim, *et al.*, "Terahertz spectral properties of PEO-based anti-adhesion films cross-linked by electron beam irradiation," Polymers **14**, 2008 (2022).
5. H. Kim, D. Kang, S. J. Oh, *et al.*, "Nondestructive evaluation on dispersion of steel fibers in UHPC using THz electromagnetic waves," Constr. Build. Mater. **172**, 293–299 (2018).
6. J.-H. Son, *Terahertz Biomedical Science and Technology* (CRC Press, 2014).
7. L. V. Titova, A. K. Ayesheshim, A. Golubov, *et al.*, "Intense THz pulses down-regulate genes associated with skin cancer and psoriasis: a new therapeutic avenue?" Sci. Rep. **3**, 2363 (2013).
8. N. Bajwa, S. Sung, D. B. Ennis, *et al.*, "Terahertz imaging of cutaneous edema: correlation with magnetic resonance imaging in burn wounds," IEEE Trans. Biomed. Eng. **64**, 2682–2694 (2017).
9. V. P. Wallace, A. J. Fitzgerald, S. Shankar, *et al.*, "Terahertz pulsed imaging of basal cell carcinoma *ex vivo* and *in vivo*," Br. J. Dermatol. **151**, 424–432 (2004).
10. A. J. Fitzgerald, V. P. Wallace, M. Jimenez-Linan, *et al.*, "Terahertz pulsed imaging of human breast tumors," Radiology **239**, 533–540 (2006).
11. Y. Bin Ji, J. M. Kim, Y. H. Lee, *et al.*, "Investigation of keratinizing squamous cell carcinoma of the tongue using terahertz reflection imaging," J. Infrared Millim. Terahertz Waves **40**, 247–256 (2019).
12. N. Vohra, T. Bowman, P. M. Diaz, *et al.*, "Pulse terahertz reflection imaging of tumors in a spontaneous model of breast cancer," Biomed. Phy. Eng. Express **4**, 065025 (2018).
13. C. B. Reid, A. Fitzgerald, G. Reese, *et al.*, "Terahertz pulsed imaging of freshly excised human colonic tissues," Phys. Med. Biol. **56**, 4333–4353 (2011).
14. S. J. Oh, S.-H. Kim, Y. B. Ji, *et al.*, "Study of freshly excised brain tissues using terahertz imaging," Biomed. Opt. Express **5**, 2837–2842 (2014).
15. A. Gavdush, N. Chernomyrdin, K. Malakhov, *et al.*, "Terahertz spectroscopy of gelatin-embedded human brain gliomas of different grades: a road toward intraoperative THz diagnosis," J. Biomed. Opt. **24**, 027001 (2019).
16. Y. B. Ji, E. S. Lee, S.-H. Kim, *et al.*, "A miniaturized fiber-coupled terahertz endoscope system," Opt. Express **17**, 17082–17087 (2009).
17. Z. Yan, L.-G. Zhu, K. Meng, *et al.*, "THz medical imaging: from *in vivo* to *in vivo*," Trends Biotechnol. **40**, 816–830 (2022).
18. C. Yu, S. Fan, and E. Pickwell-MacPherson, "The potential of terahertz imaging for cancer diagnosis: a review of investigations to date," Quant. Imaging Med. Surg. **2**, 33–45 (2012).
19. J.-H. Son, S. J. Oh, and H. Cheon, "Potential clinical applications of terahertz radiation," J. Appl. Phys. **125**, 190901 (2019).
20. J. M. Kim, I. S. Choe, K. H. Bak, *et al.*, "Surgical extent of transsphenoidal approach: a microsurgical anatomy," J. Korean. Neurosurg. Soc. **28**, 49–157 (1999).
21. G. Guizzardi, A. Mosteiro, J. Hoyos, *et al.*, "Endoscopic transorbital approach to the middle Fossa: qualitative and quantitative anatomic study," Oper. Neurosurg. **23**, e267–e275 (2022).
22. R. Wallis, R. Degl Innocenti, D. S. Jessop, *et al.*, "Investigation of hollow cylindrical metal terahertz waveguides suitable for cryogenic environments," Opt. Express **24**, 30002–30014 (2016).
23. T. Ito, Y. Matsuura, M. Miyagi, *et al.*, "Flexible terahertz fiber optics with low bend-induced losses," J. Opt. Soc. Am. B **24**, 1230–1235 (2007).
24. G. Xie, Y. Zhong, G. Li, *et al.*, "300 GHz bending transmission of silver/polypropylene hollow terahertz waveguide," Results Phys. **19**, 103534 (2020).
25. M. Mbonye, R. Mendis, and D. Mittleman, "A terahertz two-wire waveguide with low bending loss," Appl. Phys. Lett. **95**, 233506 (2009).
26. H. Bao, K. Nielsen, O. Bang, *et al.*, "Dielectric tube waveguides with absorptive cladding for broadband, low-dispersion and low loss THz guiding," Sci. Rep. **5**, 7620 (2015).
27. V. Setti, L. Vincetti, and A. Argyros, "Flexible tube lattice fibers for terahertz applications," Opt. Express **21**, 3388–3399 (2013).
28. K. Jia, L. Fan, and Z. Cao, "THz narrow band-pass filter based on stopband modulation in corrugated parallel plate waveguides," Opt. Commun. **465**, 125604 (2020).
29. E. S. Lee, J.-K. So, G.-S. Park, *et al.*, "Terahertz band gaps induced by metal grooves inside parallel-plate waveguides," Opt. Express **20**, 6116–6123 (2012).
30. S. Atakaramians, S. Afshar, M. Nagel, *et al.*, "THz porous fibers: design, fabrication and experimental characterization," Opt. Express **17**, 14053–14062 (2009).
31. Y. S. Lee, H. Choi, B. Kim, *et al.*, "Low-loss polytetrafluoroethylene hexagonal porous fiber for terahertz pulse transmission in the 6G mobile communication window," IEEE Trans. Microw. Theory Tech. **69**, 4623–4630 (2021).
32. A. Dupuis, A. Mazhorova, F. Désévédavy, *et al.*, "Spectral characterization of porous dielectric subwavelength THz fibers fabricated using a microstructured molding technique," Opt. Express **18**, 13813–13828 (2010).
33. H. Bao, K. Nielsen, H. K. Rasmussen, *et al.*, "Fabrication and characterization of porous-core honeycomb bandgap THz fibers," Opt. Express **20**, 29507–29517 (2012).
34. K. Nielsen, H. K. Rasmussen, A. J. L. Adam, *et al.*, "Bendable, low-loss Topas fibers for the terahertz frequency range," Opt. Express **17**, 8592–8601 (2009).
35. H. Park, M. Cho, J. Kim, *et al.*, "Terahertz pulse transmission in plastic photonic crystal fibres," Phys. Med. Biol. **47**, 3765 (2002).
36. S. Atakaramians, S. Afshar, T. M. Monro, *et al.*, "Terahertz dielectric waveguides," Adv. Opt. Photon. **5**, 169–215 (2013).
37. I. Elgali, O. Omar, C. Dhlin, *et al.*, "Guided bone regeneration: materials and biological mechanisms revisited," Eur. J. Oral Sci. **125**, 315–337 (2017).
38. S. J. Oh, S.-H. Kim, K. Jeong, *et al.*, "Measurement depth enhancement in terahertz imaging of biological tissues," Opt. Express **21**, 21299–21305 (2013).
39. K. Oh and U. C. Paek, *Silica Optical Fiber Technology for Devices and Components: Design, Fabrication, and International Standards* (Wiley, 2012).

40. A. V. Velamuri, K. Patel, I. Sharma, *et al.*, "Investigation of planar and helical bend losses in single-and few-mode optical fibers," J. Lightwave Technol. **37**, 3544–3556 (2019).
41. J. A. Jacques, *Beam and Fiber Optics* (Elsevier, 2012).
42. Z. Vilagosh, A. Lajevardipour, and A. W. Wood, "Computational absorption and reflection studies of normal human skin at 0.45 THz," Biomed. Opt. Express **11**, 417–431 (2020).
43. M. Midrio and M. P. Singh, "The space-filling mode of holey fibers: an analytical vectorial solution," J. Lightwave Technol. **18**, 1031–1037 (2000).
44. B. You, C.-Y. Chen, C.-P. Yu, *et al.*, "Frequency-dependent skin penetration depth of terahertz radiation determined by water sorption–desorption," Opt. Express **26**, 22709–22721 (2018).
45. J. Y. Suen and W. J. Padilla, "Superiority of terahertz over infrared transmission through bandages and burn wound ointments," Appl. Phys. Lett. **108**, 233701 (2016).
46. M. Naftaly, R. E. Miles, and P. J. Greenslade, "THz transmission in polymer materials—a data library," in *Proceedings of IEEE 32th International Conference on Infrared, Millimeter, and Terahertz Waves* (2007), pp. 819–820.
47. M. S. Hossain, S. Sen, and M. M. Hossain, "Reduction of effective material loss (EML) using decagonal photonic crystal fiber (D-PCF) for communication applications in the terahertz wave pulse," Opt. Quantum Electron. **54**, 658 (2022).
48. https://www.zeusinc.com/.
49. https://www.fospia.com/.
50. T. Martynkien, J. Olszewski, M. Szpulak, *et al.*, "Experimental investigations of bending loss oscillations in large mode area photonic crystal fibers," Opt. Express **15**, 13547–13556 (2007).
51. J. Han, E. Liu, and J. Liu, "Circular gradient-diameter photonic crystal fiber with large mode area and low bending loss," J. Opt. Soc. Am. A **36**, 533–539 (2019).